arXiv:1406.5968v1 [astro-ph.HE] 23 Jun 2014

Detection of high velocity outflows in Seyfert 1 *Mrk 590*

A. Gupta[1,2], S. Mathur[2], Y. Krongold[3]

ABSTRACT

We report on the detection of ultra-fast outflows in the Seyfert 1 galaxy *Mrk 590*. These outflows are identified through highly blue-shifted absorption lines of O VIII & Ne IX in the medium energy grating spectrum and Si XIV & Mg XII in the high energy grating spectrum on board *Chandra* X-ray observatory. Our best fit photoionization model requires two absorber components at outflow velocities of 0.176c and 0.0738c and a third tentative component at 0.0867c. The components at 0.0738c and 0.0867c have high ionization parameter and high column density, similar to other ultra-fast outflows detected at low resolution by Tombesi et al. These outflows carry sufficient mass and energy to provide effective feedback proposed by theoretical models. The component at 0.176c, on the other hand, has low ionization parameter and low column density, similar to those detected by Gupta et al. in Ark 564. These absorbers occupy a different locus on the velocity vs. ionization parameter plane and have opened up a new parameter space of AGN outflows. The presence of ultra-fast outflows in moderate luminosity AGNs poses a challenge to models of AGN outflows.

1. Introduction

Outflows are ubiquitous in AGNs, manifested by high-ionization absorption lines in X-rays and UV (Mathur et al. 1995; 1997, and references therein). The X-ray absorbers, commonly known as warm absorbers (WAs), have typical outflow velocities of $100-1000$ km s^{-1}. The discovery of ultra-fast outflows (UFOs) at velocities $v \sim 0.1c$ in the hard X-ray band has added an intriguing aspect to the rich field of AGN outflows. These outflows are exhibited by blueshifted absorption lines, produced mostly by highly ionized iron (Pounds et al. 2003a;b,

[1]Department of Biological and Physical Sciences, Columbus State Community College, Columbus, OH 43215, USA; agupta1@cscc.edu

[2]Department of Astronomy, The Ohio State University, 140 West 18th Avenue, Columbus, OH 43210, USA

[3]Instituto de Astronomia, Universidad Nacional Autonoma de Mexico Mexico City, (Mexico)

Tombesi et al. 2010, and references therein). The mass outflow rate of UFOs can be comparable to the accretion rate and their kinetic energy can correspond to a significant fraction of the bolometric luminosity (Tombesi et al. 2013, Pounds et al. 2003a;b, Reeves et al. 2009). Thus these outflows can provide effective feedback that is required by theoretical models of galaxy formation (e.g., Hopkins & Elvis 2010, Silk & Rees 1998).

While WAs are detected unambiguously in the high-resolution soft X-ray spectra and their physical properties and kinematics are well determined (e.g., Krongold et al. 2003), the same cannot be said about UFOs. The UFOs in *PG 1211+143* and *PG 0844+349* (Pounds et al. 2003a;b) were detected in high-resolution grating spectra, but the rest of the UFOs are detected in low-resolution CCD spectra, observed with the *XMM-Newton* and *Suzaku* . The rest frame energy of the Fe-Kα line transition is 6.38 keV, and at outflow velocity of $\approx$ 0.1c the UFOs are observed at about 7.0 keV. This falls in the region of the spectrum where the effective area and resolution are low. As a result the significance of the absorption line detection in the hard X-ray band is often questioned (e.g., Laha et al. 2014) and with only a few lines observed, accurate parameterization of the photoionized plasma becomes difficult. These difficulties were alleviated with our discovery of relativistic outflows in the soft X-ray band in high-resolution spectra.

We recently discovered relativistic outflows in *Chandra* HETG spectra of Seyfert 1 galaxy *Ark 564* (Gupta et al. 2013b); these detections are robust, with high statistical significance. We identified highly blueshifted absorption lines of O VI, O VII and O VIII and successfully fitted them with a two-component photo-ionization model. The detection of multiple lines at the same velocity makes the identification of the relativistic outflow robust. This opens up an exciting new opportunity of probing the relativistic disk winds in the soft X-ray band where we have the best diagnostic power from multiple lines of multiples ionization states of several elements and where the gratings response is the best.

Excited by the discovery of relativistic outflows in *Ark 564*, we looked for their presence in other AGNs; could it be that they were not found because nobody looked for them? The Chandra HETGS data of *Mrk 590* are tantalizing. *Mrk 590* is a bright Seyfert 1 galaxy (recently appears to have changed from Type 1 to Type $\sim 1.9-2$; Denney et al. 2014) at $z = 0.026$ that has been observed by the Einstein observatory (Kriss et al. 1980), the HEAO 1 (Piccinotti et al. 1982), the *BATSE* (Malizia et al. 1999) and recently by *Chandra* and *XMM-Newton* . Gallo et al. (2006) first reported the presence of a strong Fe K emission line revealed in the 2002 $\sim$ 10 ks *XMM-Newton* EPIC data. Later Longinotti et al. (2007) presented its complex spectrum with a reflection component using the $\sim$ 100 ks observations with *Chandra* and *XMM-Newton* and confirmed the presence of the Fe Kα emission line. Here we present a detailed reanalysis of the *Chandra* HETG observation of *Mrk 590*.

2. Observation and data reduction

Mrk 590 was observed by *Chandra* High Energy Transmission Grating (HETG) in 2004 for $\sim 100\ ks$ (ObsID: 4924). The HETG is comprised of two gratings: the medium energy gratings (MEG) and the high energy gratings (HEG), which disperse spectra into positive and negative spectral orders. We reduced the data for both gratings using the standard Chandra Interactive Analysis of Observations (CIAO) software (v4.3) and Chandra Calibration Database (CALDB, v4.4.2) and followed the standard Chandra data reduction threads[1]. To increase S/N we co-added the negative and positive first-order spectra and built the effective area files (ARFs) using the *fullgarf* CIAO script.

3. Spectral Analysis

For the spectral analysis, we binned the MEG and HEG spectra to their resolution element of 0.025 $\mathring{A}$ and 0.012 $\mathring{A}$ respectively and analyzed using the CIAO fitting package *Sherpa*. Throughout this paper the quoted errors correspond to 1 σ significance.

3.1. Continuum Modeling

We fit the intrinsic continuum of the source with an absorbed (Galactic $N_H = 2.7 \times 10^{20}\ cm^{-2}$; Dickey & Lockman 1990) powerlaw; the fit parameters are reported in the Table 1. In the energy band of $0.3 - 10\ keV$, the integrated flux is $9.1 \times 10^{-12}\ ergs\ s^{-1}\ cm^{-2}$, which corresponds to an unabsorbed X-ray luminosity of $1.4 \times 10^{43}\ ergs\ s^{-1}$.

Although absorbed powerlaw fits the continuum well (MEG: $\chi^2 = 729, d.o.f. = 679$, HEG: $\chi^2 = 1120, d.o.f. = 1199$), there are residual absorption line-like features in the spectral regions of $10 - 20$ Å and $4 - 9$ Å in the MEG and HEG spectra respectively (Fig. 1 & 2). In the subsequent sections we discuss the identification, statistical significance and possible origin of these absorption lines.

[1] `http://cxc.harvard.edu/ciao/threads/index.html`

3.2. Identification of the Absorption Lines

3.2.1. Medium Energy Grating Spectrum

In the MEG spectrum of *Mrk 590* the most prominent absorption feature ($> 3\sigma$; Fig. 3) is present at 16.03 Å. Addition of a gaussian absorption feature (at 16.033 ± 0.004) to continuum model improves the fit ($\Delta\chi^2 = 17$ for 2 fewer d.o.f.) at the confidence level of 99.97% according to the F-test (Bevington & Robinson 1992). The measured equivalent width (EW) is 46.50 ± 11.04 mÅ. Errors are at 1σ confidence level and are calculated using the "projection" command in *Sherpa*. According to the Gaussian probability distribution the probability of detecting the line by chance is 1.3×10^{-5}. There are 681 wavelength bins in the MEG spectrum, so the probability of finding an absorption line at the observed significance anywhere in the spectrum due to random statistical fluctuations is 0.88%. Thus it is highly unlikely that this absorption feature is due to random statistical fluctuations.

We tried to identify the absorption feature detected at 16.033 ± 0.004 Å. There is no known instrumental feature near this energy (Chandra Proposers Observatory Guide, or POG). Though this line could be associated with $z = 0$ O VIII Kβ line ($\lambda_{rest} = 16.007$ Å), we rule out this possibility because there is no corresponding O VIII Kα line ($\lambda_{rest} = 18.967$Å). Assuming this feature is produced by Fe XVII ($\lambda_{rest} = 15.015$Å) ions in an intervening warm-hot intergalactic medium (WHIM; Mathur et al. 2003, Nicastro et al. 2005), the system redshift would be $z_{WHIM} = 0.066$ which is greater than the $z_{AGN} = 0.02638$. Thus this feature could not be from an intervening WHIM system and no other intervening absorption line is likely either. Therefore we assume that this absorption line is intrinsic to the source.

We identify this line based on a combination of chemical abundance, line strength and assuming a very broad range of inflow/outflow velocities of $\pm 60,000$ km s^{-1}. The likely candidates for the $\sim 16.033\mathring{A}$ feature are Fe XVII ($\lambda_{rest} = 15.015\ \mathring{A}$; $\lambda_s = 15.411\ \mathring{A}$, wavelength at the source redshift) with inflow velocity of $\sim 0.04c$, or O VIII ($\lambda_{rest} = 18.96\mathring{A}$; $\lambda_s = 19.460\ \mathring{A}$) with outflow velocity of $0.176 \pm 0.001c$. To distinguish between the two possibilities of inflow and outflow, we search for possible associations of other lines. We do not find any possible association for inflows but found a 2.8σ line at 11.39 ± 0.01 corresponding to Ne IX ($\lambda_{rest} = 13.447\mathring{A}$; $\lambda_s = 13.802\ \mathring{A}$, Fig. 3) at the similar outflow velocity of $0.175 \pm 0.001c$.

3.2.2. High Energy Grating Spectrum

In the *Mrk 590* HEG spectrum, we detected two absorption features at 5.80 $\mathring{A}$ and 5.88 $\mathring{A}$ (Fig. 4) with EW of 25.0 ± 4.4 mÅ and 21.4 ± 3.2 mÅ respectively. The HEG and MEG overlap in this wavelength range, so if real, these lines should also be present in the MEG spectrum. We searched for these absorption features in the MEG spectrum and found one at 5.91 ± 0.04 Åwith EW of 25.3 ± 12.5 mÅ; this is consistent with the 5.880 ± 0.001 ÅHEG line, though the error on the line EW in the MEG spectrum is large. There is no absorption feature in the MEG spectrum corresponding to the 5.80 $\mathring{A}$ HEG feature, but again the EW limit in the MEG spectrum is large, 13.13mÅ, so the discrepancy is less than 2σ. In the following we will treat both of these features as real lines, but keeping in mind that our confidence in the 5.80 $\mathring{A}$ feature is not as strong as that in the 5.88 $\mathring{A}$ feature.

In the HEG spectrum, both lines are present at high significance with a very low probability of finding them by chance (3×10^{-4}% and 6×10^{-5}%) anywhere in the spectrum. The only possible identification we found for them is of Si XIII and Si XIV at outflow velocities of $0.085c$–$0.067c$. We will see later that the photo-ionization model supports the identification of these lines as Si XIV .

4. Photo-ionization model: fitting with PHASE

To test the validity of our tentative identifications of absorption features with high-velocity outflows, we fitted them with our photo-ionization model code PHASE (Krongold et al. 2003). The code has 4 free parameters per absorbing component, namely 1) the ionization parameter $U = \frac{Q(H)}{4\pi r^2 n_H c}$; where *Q(H)* is the rate of H ionizing photons, r is the distance to the source, n_H is the hydrogen number density and c is the speed of light; 2) the hydrogen equivalent column density N_H; 3) the outflow velocity of the absorbing material V_{out} and 4) the micro-turbulent velocity V_{turb} of the material. PHASE has the advantage of producing a self-consistent model for each absorbing component, because the code starts without any prior constraint on the column density or ionization fraction of any ion. We have assumed solar elemental abundances (Grevesse et al. 1993) in the following analysis.

The residual features at 16.033 ± 0.004 and 11.39 ± 0.01 in the MEG spectrum are well fitted with one PHASE component of $\log U = -0.10 \pm 0.25$ and $\log N_H = 20.2 \pm 0.2$ and outflow velocity of $0.176 \pm 0.001c$ (Fig. 5) and the lines are indeed O VIII Kα and Ne IX . The addition of the PHASE component to the continuum model significantly improves the fit ($\Delta\chi^2 = 15$ for 3 fewer d.o.f.). According to F-test, the absorber is present at a confidence level of 99.66%. We call this component as the high-velocity–low-ionization-phase (HV-LIP)

absorber. Our best fit absorber model also predicts absorption from O VII at 18.26 Å. As shown in figure 5, the data are consistent with the prediction. However, to securely detect the O VII feature, we require higher signal to noise data.

To model the HEG absorption features (at 5.08 $\mathring{A}$ and 5.88 $\mathring{A}$) identified as Si XIII or Si XIV , required two PHASE components with $\log U = 2.5 \pm 0.3$ and $\log N_H = 23.50 \pm 0.03$ at different outflow velocities (Fig. 6). The photo-ionization model fitting favors the identification of these features as ionic transition of Si XIV produced in highly ionized medium outflowing with velocity of $0.0867 \pm 0.0007c$ and $0.0738 \pm 0.0004c$ respectively. Both the absorbers are required at high significance of 99.999% ($\Delta\chi^2 = 24$ for 4 fewer d.o.f.) and 99.996% ($\Delta\chi^2 = 28$ for 4 fewer d.o.f.) respectively. The HEG best fit model with two absorbers also requires Mg XII absorption features at 7.90 and 8.01 $\mathring{A}$; these lines are in fact present and are well fitted by the model. The best fit PHASE parameters are reported in Table 2 and the best fit models are shown in Fig. 6. These absorbers fit the high ionization lines, so we will refer to these absorbers as the high-velocity–high-ionization phase I (HV-HIP-I) and high-velocity–high-ionization phase II (HV-HIP-II) components. Successfully modeling the residuals in the MEG and HEG spectra further supports the presence of high-velocity outflows in *Mrk 590*.

5. Mass and Energy ouflow rate estimates

Without knowing the location of the absorber, its mass and energy outflow rates cannot be well constrained. The lower limit on the absorber location can be determined assuming that the observed outflow velocity is the escape velocity at the launch radius r: i.e. $r = \frac{2GM_{BH}}{v_{out}^2}$. Peterson et al. (2004) determine the central black hole mass of *Mrk 590* to be $M_{BH} = (4.75 \pm 0.74) \times 10^7 M_\odot$. Using the above expression we get the minimum distance of *Mrk 590* HV-LIP and HV-HIP absorbers of $\sim 1.5 \times 10^{-4}$ pc and $\sim 6.1 \times 10^{-4}$ pc respectively. This is 0.17 and 0.72 light-days from the nuclear black hole, and inside the broad emission line region.

For a bi-conical wind, the mass outflow rate is $\dot{M}_{out} \approx 1.2\pi m_p N_H v_{out} r$ (Krongold et al. 2007). Substituting r with r_{min} and using outflow velocities of 52800 km s^{-1} and 26010 km s^{-1}, we obtain lower limit on mass outflow rates of $\dot{M}_{out} \geq 3.8 \times 10^{-5}$ M$_\odot$ s^{-1} and $\dot{M}_{out} \geq 1.5 \times 10^{-1}$ M$_\odot$ s^{-1}, respectively. These corresponds to kinetic luminosity of LIP and HIP high velocity outflows of $\dot{E}_K \geq 1.1 \times 10^{41}$ erg s^{-1} and $\dot{E}_K \geq 2.2 \times 10^{44}$ erg s^{-1}, respectively. The kinetic luminosity of HIP high velocity outflows is much larger than X-ray (2-10 keV) luminosity of 7.0×10^{42} erg s^{-1}. Thus in principle these outflows have the potential to provide effective feedback.

6. Discussion

The *Chandra* observation of *Mrk 590* has revealed low- and high-ionization high-velocity outflows. The low-ionization and low-column (HV-LIP) component is similar to those recently discovered in another Seyfert-type moderate luminosity AGN *Ark 564* (Gupta et al. 2013b). However, the outflows identified as HV-HIP-I and HV-HIP-II have parameters similar to that of UFOs (highly ionized $log\xi = 3 - 6$ erg s^{-1} and with large column densities $N_H = 10^{22} - 10^{24}$ cm^{-2}).

Recently Tombesi et al. (2013) presented the connection between UFOs and soft X-ray WAs. They strongly suggest that these absorbers represent parts of a single large-scale stratified outflow and that they continuously populate the whole parameter space (ionization, column, velocity), the WAs and the UFOs lying at the two ends of the distribution (Fig. 7). The *Ark 564* low-velocity WAs (Gupta et al. 2013a) and UFOs (Papadakis et al. 2007) were in agreement with the linear correlation fits from Tombesi et al., but the low-ionization low-column high-velocity outflows in *Ark 564* probe a completely different parameter space (U, N_H, v_{out}), as shown in Fig.7. Similarly the *Mrk 590* HV-HIP outflows probe the same parameter space as of UFOs, but HV-LIP outflows probe the parameter space not covered by either low-velocity WAs or high-ionization UFOs.

The presence of different absorption systems with different outflow velocities may suggest that we are looking at the flows in a transverse configuration with respect to the line of sight. This would avoid possible collision between different components, that would result in shock-heating of the gas and a decrease on the measured opacity. The geometry would have to be conical and the flows must form a large angle with the accretion disk. It is also expected that the orthogonal component of the velocity might have a significant contribution to the total velocity of the flow, but we only observe the component in the line of sight. This would mean that the flows are even faster than detected. In such a steady state configuration, the absorption lines could be expected to remain constant over time, as we would always observe the same section of the wind.

Alternatively, we may be seeing a radial flow, with a nearly spherical geometry and a large velocity gradient in the line of sight. The different velocity components could be explained if they are parts of this single flow, formed by clumps in the flow. In this scenario, strong variability in the observed absorption lines is expected, as the clumps move further out from the central engine, and their velocity and ionization state change. Observations of *Mrk 590* over time would allow us to discriminate between these two scenarios.

As discussed in Gupta et al. (2013b), the relativistic outflows cannot be explained by simple models of radiation pressure driven winds. Their velocities are too large for their

luminosities and magneto-hydrodynamics may be involved. Magnetic fields are also important for launching jets; could relativistic outflows be failed jets? To get the in-depth view of the AGN outflows, its important to search for more of such systems probing the complete parameter space.

7. Summary

We have detected high-velocity outflows in the Seyfert 1 galaxy *Mrk 590*. These absorbers are identified through highly blue-shifed absorption lines of O VIII & Ne IX in the MEG spectrum and Si XIV & Mg XII in the HEG spectrum. Our best fit photoionization model requires three absorber components at outflow velocities of 0.176c, 0.0867c and 0.0738c. The HV-LIP absorber has low -ionization and -column density while two HV-HIP absorbers have high -ionization and -column density. All the absorbers are required at high significance of 99.66%, 99.999% and 99.996% respectively. The HV-HIPs have sufficient mass and energy to provide effective feedback proposed by theoretical models. However, the presence of such UFOs in moderate-luminosity AGNs poses a challenge to models of AGN winds.

REFERENCES

Bevington, P.R. & Robinson, D.K. 1992, New York: McGraw-Hill, 2nd ed.

Denney, K. D., De Rosa, G., Croxall, K., Gupta, A. et al. 2014, arXiv:1404.4879

Gallo, L. C., Lehmann, I., Pietsch, W. et al. 2006, MNRAS, 365, 688

Grevesse, N., Noels, A., & Sauval, A. J. 1993, A&A, 271, 587

Gupta, A., Mathur, S., Krongold, Y., & Nicastro, F. 2013, ApJ, 768, 141

Gupta, A., Mathur, S., Krongold, Y., & Nicastro, F. 2013, ApJ, 772, 66

Hopkins, P. & Elvis, M. MNRAS, 401, 7

Kriss, G. A., Canizares, C. R., & Ricker, G. R. 1980, ApJ, 242, 492

Krongold, Y., Nicastro, F., Brickhouse, N.S., Elvis, M., Liedahl D.A. & Mathur, S. 2003, ApJ, 597, 832

Krongold, Y., Nicastro, F., Elvis, M. et al. 2007, ApJ, 659, 1022

Laha, S., Guainazzi, M., Dewangan, G.C. et al. 2014, arXiv1404.0899

Longinotti, A. L., Bianchi, S., Santos-Lleo, M. et al. 2007, å, 470, 73

Malizia, A., Bassani, L., Zhang, S. N. et al. 1999, ApJ, 519, 637

Mathur, S., Elvis, M., & Wilkes, B. 1995, ApJ, 452, 230

Mathur, S., Wilkes, B. & Aldcroft, T. 1997, ApJ, 478, 182

Mathur,S., Weinberg, D.H., & Chen, X. 2003,ApJ, 582, 82

Nicastro, F., et al. 2005, *nature*, 433, 49

Papadakis, I. E., Brinkmann, W., Page, M. J., McHardy, I., & Uttley, P. 2007, A&A, 461, 931

Peterson, B. M., Ferrarese, L., Gilbert, K. M. et al. 2004, ApJ, 613, 682

Piccinotti, G., Mushotzky, R. F., Boldt, E. A. et al. 1982, ApJ, 253, 485

Pounds, K. A. et al. 2003, MNRAS, 345, 705

Pounds, K. A. et al. 2003, MNRAS, 346, 1025

Reeves, J. N. et al. 2009, ApJ, 701, 493

Silk, J. & Rees, M.J. 1998, A&A, 331, 1

Tombesi, F. et al. 2008, A&A, 521, 57

Tombesi, F. et al. 2013, MNRAS, 430, 110

This preprint was prepared with the AAS LaTeX macros v5.2.

Table 1. Continuum model parameters for the Mrk590 *Chandra* HETG spectra

	Units	MEG	HEG
Powerlaw			
Photoindex (Γ)		1.57 ± 0.03	1.56 ± 0.03
Normalization	$10^{-4}\ ph\ keV^{-1}\ s^{-1}\ cm^{-2}$	15.84 ± 0.25	13.36 ± 0.37

Table 2. Absorption lines identified with high velocity outflows in the HETGS Spectrum of Mrk 590.

Ion	λ_{obs} Å	λ_{rest} Å	v_{out} km s^{-1}	EW mÅ
Medium Energy Grating				
O VIII $K\alpha$	16.033 ± 0.004	18.969	52936 ± 62	46.50 ± 11.04
Ne IX	11.39 ± 0.01	13.447	52423 ± 217	20.7 ± 7.48
High Energy Grating				
Si XIV	5.804 ± 0.003	6.182	25584 ± 141	25.0 ± 4.4
Si XIV	5.880 ± 0.001	6.182	21990 ± 47	21.4 ± 3.2

Table 3. Best fit photoionization model parameters.

	MEG	HEG	
Parameter	HV-LIP	HV-HIP-I	HV-HIP-II
Log U	-0.1 ± 0.2	2.5 ± 0.2	2.5 ± 0.2
Log N_H (cm^{-2})	20.2 ± 0.2	23.5 ± 0.3	23.5 ± 0.2
V_{Turb} ($\mathrm{km\ s}^{-1}$)	303 ± 41	688 ± 123	890 ± 112
V_{Out} ($\mathrm{km\ s}^{-1}$)	52800 ± 300	26010 ± 210	22140 ± 120
$\Delta\chi^{2}$[a]	11	24	10

[a] Improvement in χ^2 to fit after adding model component

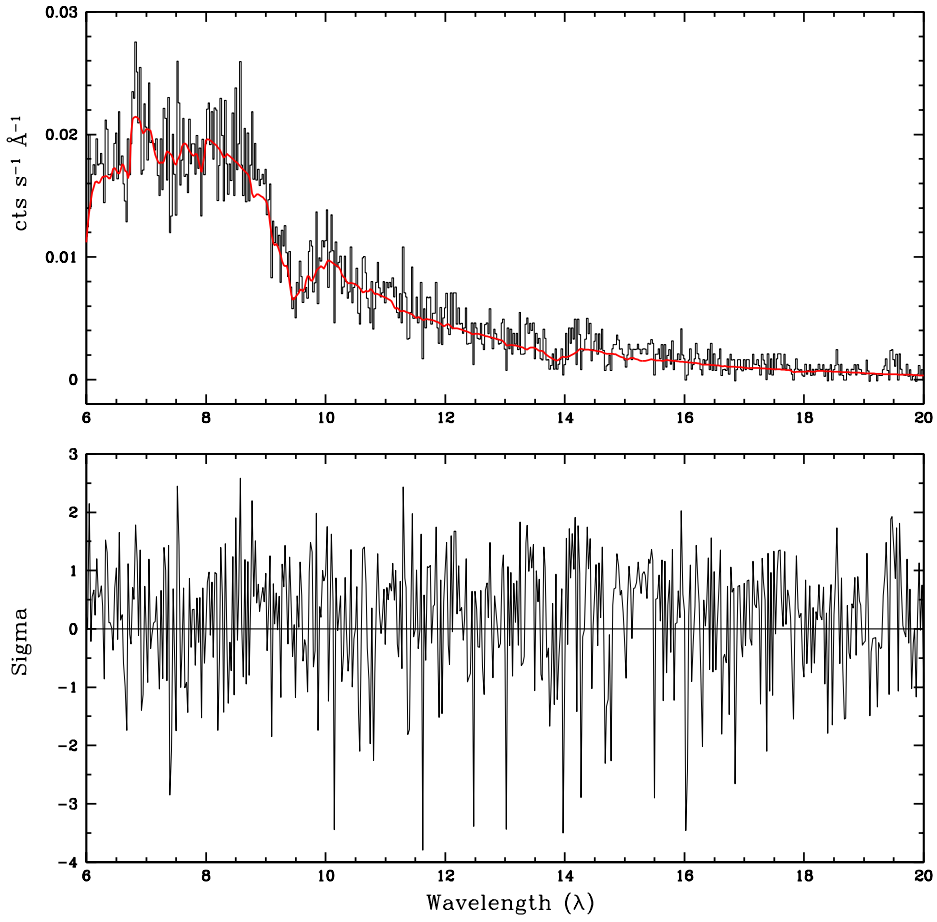

Fig. 1.— The Mrk 590 MEG spectrum in the observer frame. The red line shows the best fit continuum model. In the bottom panel, plotted are the residuals showing absorber features.

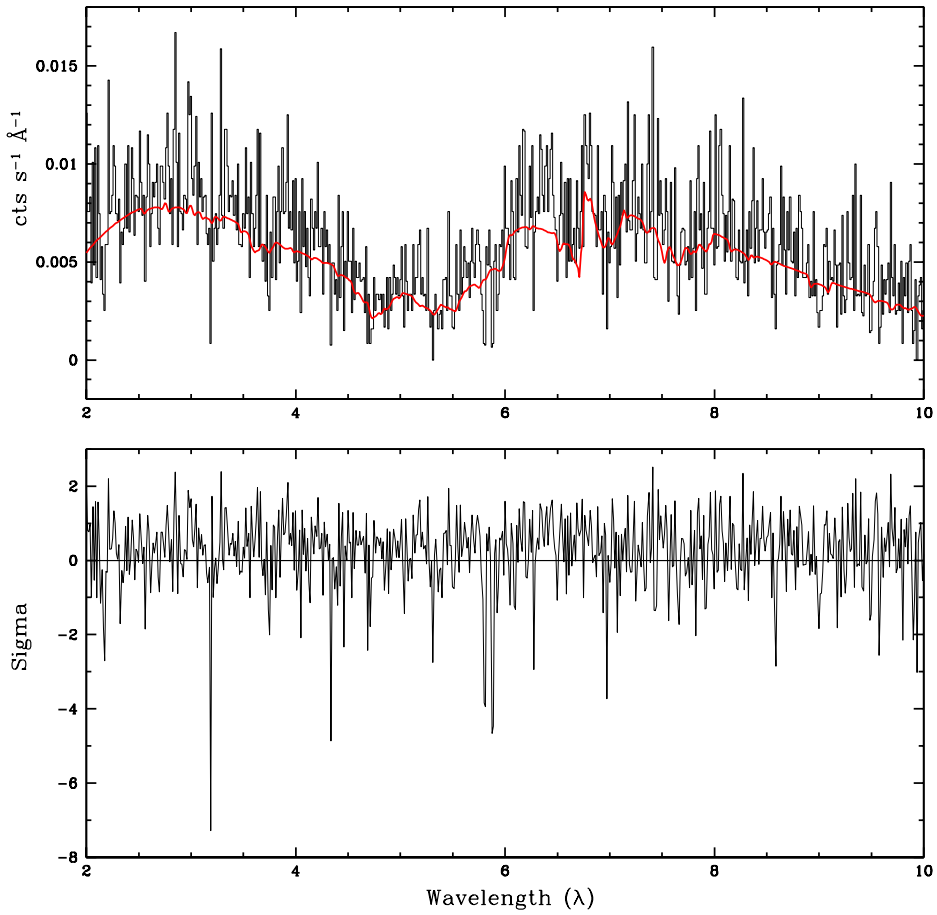

Fig. 2.— Same as fig. 1 for HEG spectrum.

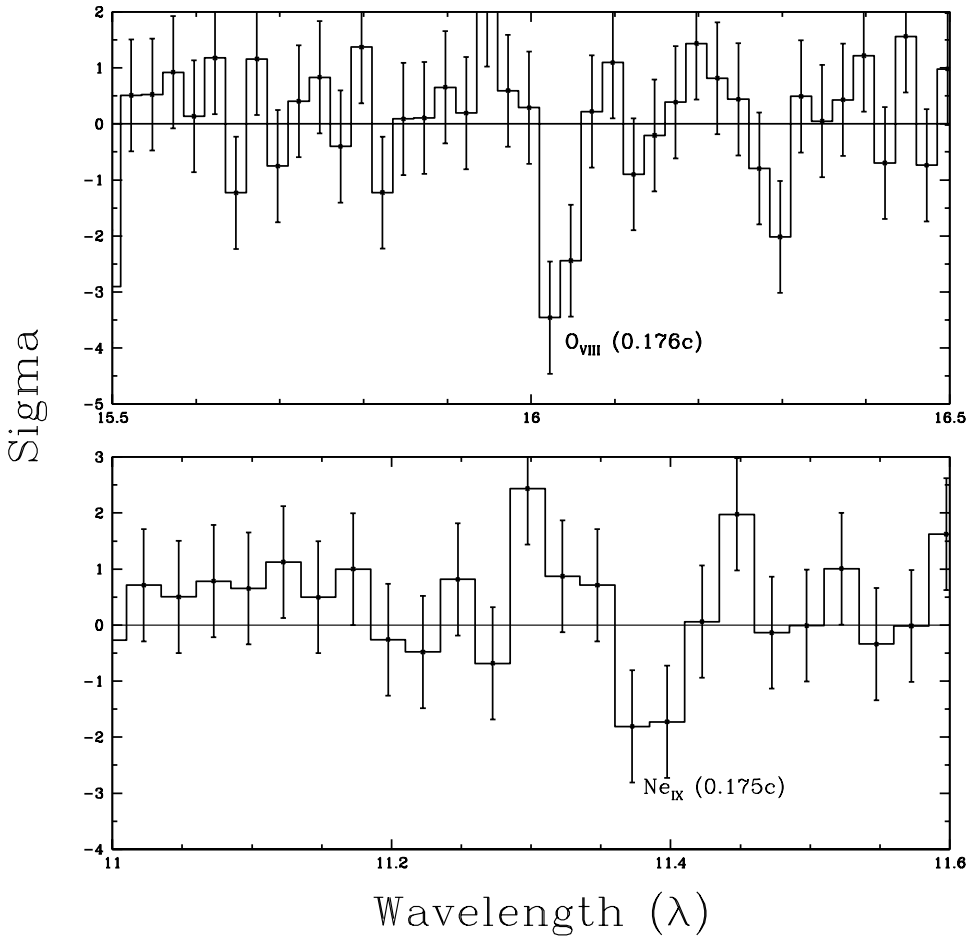

Fig. 3.— Showing the high significance residuals of data:continuum fit to the MEG spectrum of Mrk 590, in the observer frame.

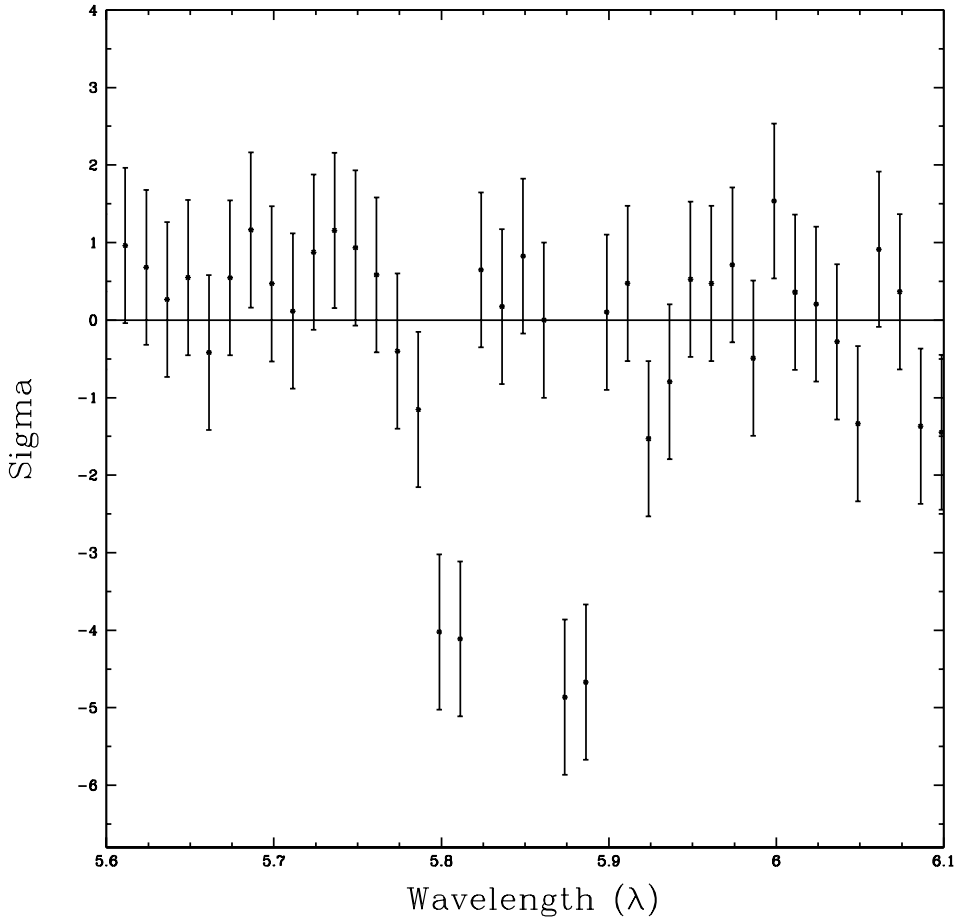

Fig. 4.— Same as fig. 3 for HEG data.

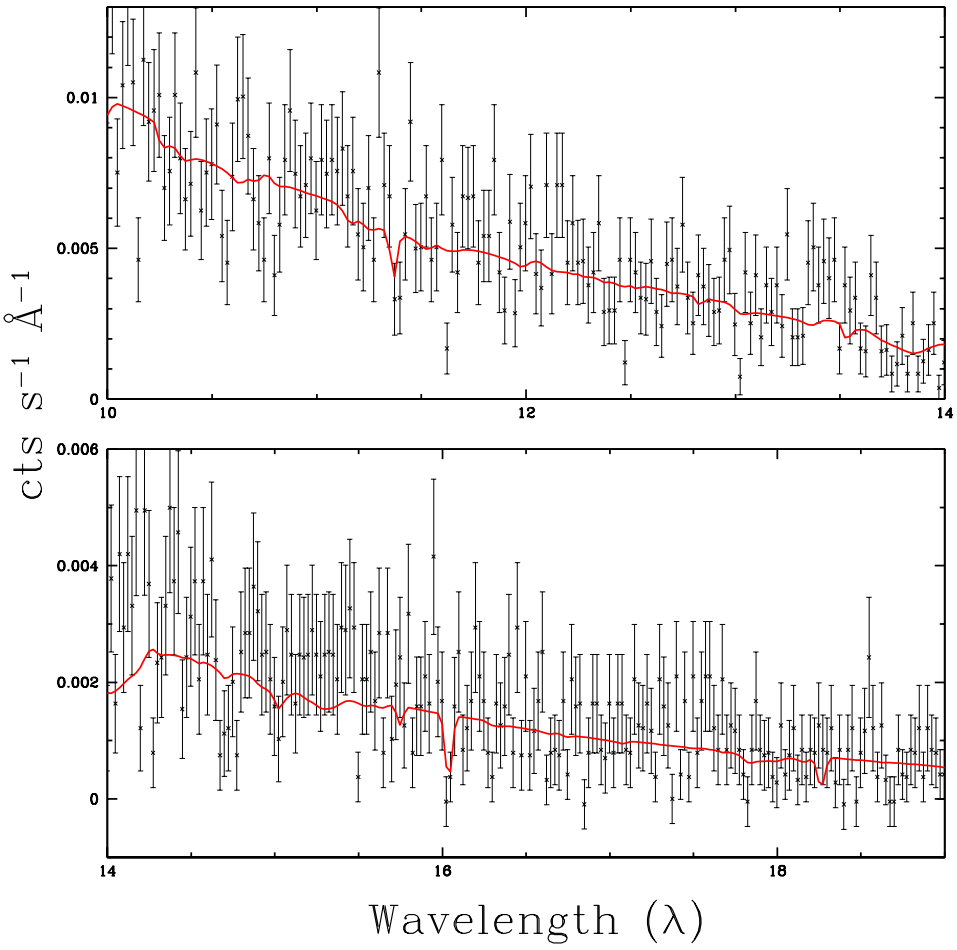

Fig. 5.— The red solid line shows the best fit absorber model at outflow velocity of 0.176c.

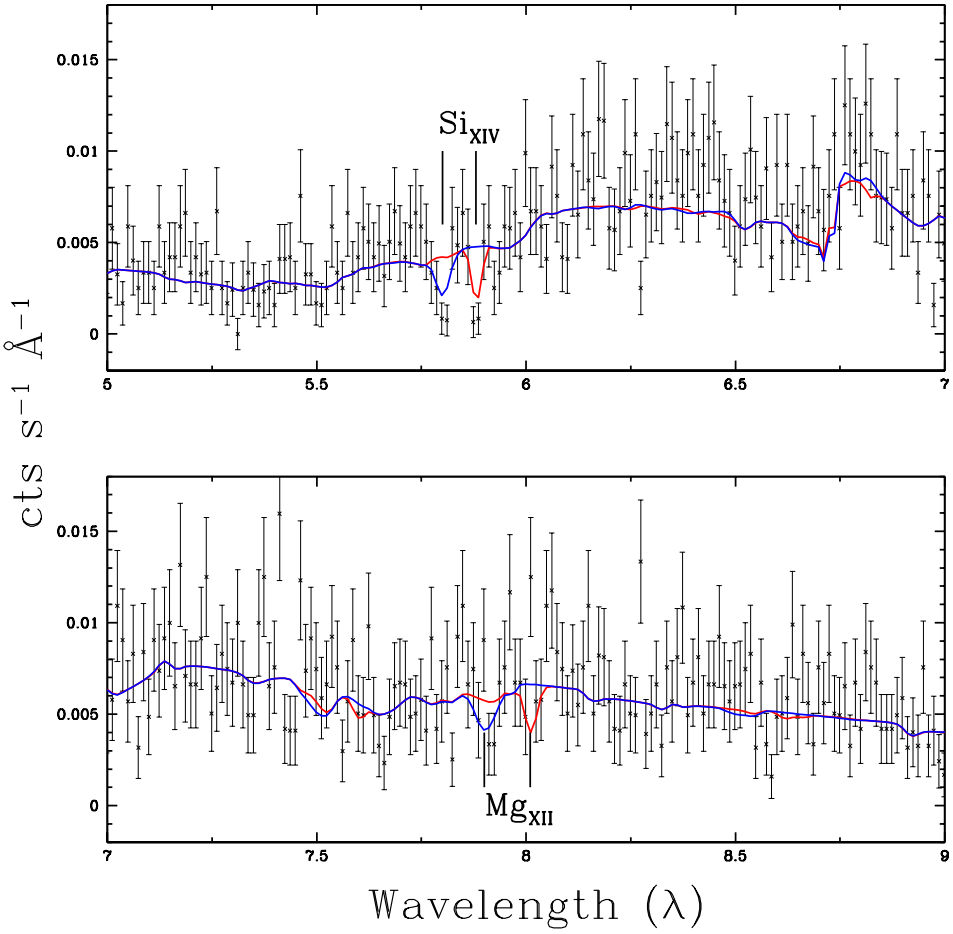

Fig. 6.— The red and blue lines show the best fit absorber models at outflow velocities of $0.0867c$ and $0.0738c$, respectively.

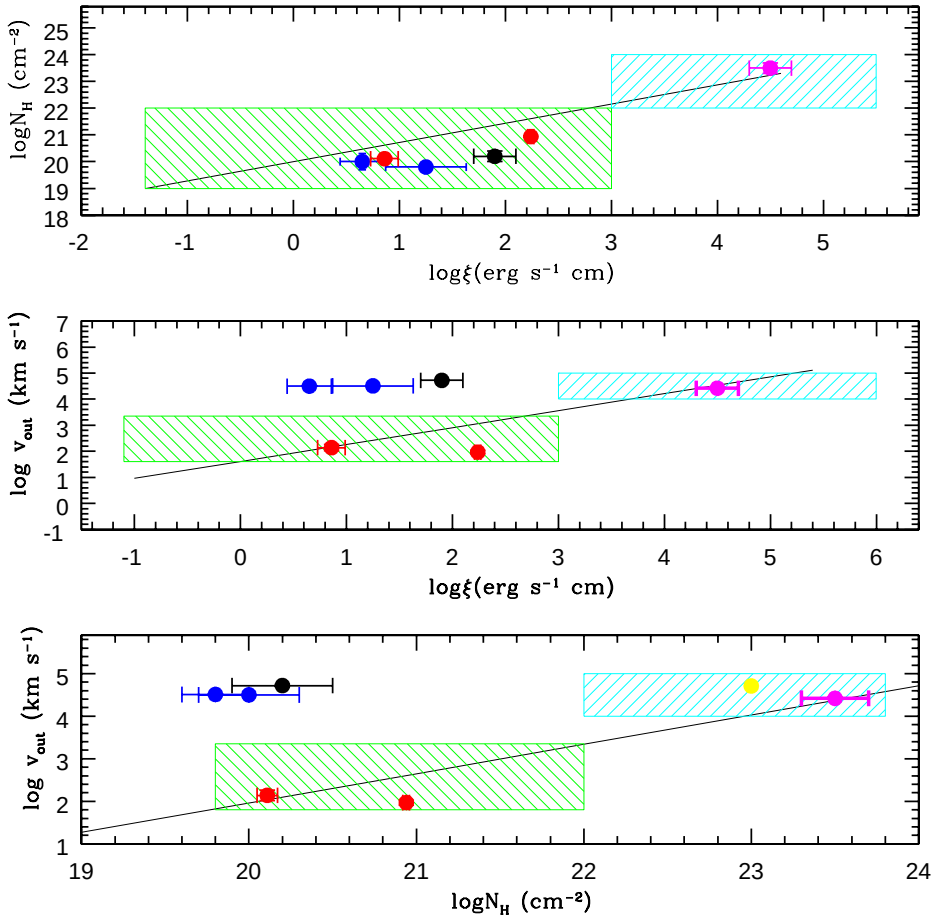

Fig. 7.— The $\log \xi$ vs. $\log N_H$ (top panel), $\log \xi$ vs. $\log v_{out}$ (middle panel) and $\log N_H$ vs. $\log v_{out}$ (bottom panel) for the low-velocity WAs (green striped region) and UFOs (blue striped region) using data from Tombesi et al. (2013). The solid lines represent the correlation fits to low-velocity WAs and UFOs from Tombesi et al. The data-points represent the Mrk 590 and Ark 564 outflow parameters, (1) Mrk 590: LIP High-velocity outflows (black) and HIP high-velocity outflows (magenta) (2) Ark 564: low-velocity WAs (red; Gupta et al. 2013a), UFO (yellow; Papadakis et al. 2007) and high-velocity outflows (blue; Gupta et al. 2013b). As we see, the high-velocity low-ionization absorbers in Ark 564 and Mrk 590 occupy an unexplored region of the parameter space.